Journal of Molecular Catalysis A: Chemical 299 (2009) 60–67

Contents lists available at ScienceDirect

Journal of Molecular Catalysis A: Chemical

journal homepage: www.elsevier.com/locate/molcata

Hydrothermally fabricated single-crystalline strontium-substituted lanthanum manganite microcubes for the catalytic combustion of toluene

Jiguang Deng[a], Lei Zhang[a], Hongxing Dai[a,*], Hong He[a], Chak Tong Au[b,**]

[a] Laboratory of Catalysis Chemistry and Nanoscience, Department of Chemistry and Chemical Engineering, College of Environmental and Energy Engineering, Beijing University of Technology, Beijing 100124, China
[b] Department of Chemistry, Hong Kong Baptist University, Kowloon Tong, Hong Kong, China

ARTICLE INFO

Article history:
Received 26 April 2008
Received in revised form
30 September 2008
Accepted 6 October 2008
Available online 14 October 2008

Keywords:
Single-crystalline perovskite-type oxide
Microcube
Toluene oxidation
Volatile organic compounds
Hydrothermal synthesis

ABSTRACT

$La_{1-x}Sr_xMnO_{3-\delta}$ ($x = 0.4$, 0.5, and 0.6) catalysts were fabricated hydrothermally from $KMnO_4$, $MnCl_2$ ($KMnO_4/MnCl_2$ molar ratio = 3/7), and stoichiometric amounts of lanthanum and strontium nitrates in KOH solution. The physicochemical properties of the materials were characterized by a number of analytical techniques. It was found that the $La_{1-x}Sr_xMnO_{3-\delta}$ samples fabricated at 250 °C are single-crystalline perovskite-type oxides in the form of microcubes. The as-fabricated $La_{1-x}Sr_xMnO_{3-\delta}$ materials display various states of oxygen nonstoichiometry. The total amount of oxygen vacancies and Mn^{4+} in the catalysts decreases in the order of $La_{0.5}Sr_{0.5}MnO_{3-\delta} > La_{0.4}Sr_{0.6}MnO_{3-\delta} > La_{0.6}Sr_{0.4}MnO_{3-\delta}$. It has been found that the trends of catalyst reducibility and catalytic performance of the three catalysts follow a similar order. We observed 100% toluene conversion at 255 °C over the $La_{0.5}Sr_{0.5}MnO_{3-\delta}$ catalyst, 113 °C lower than that observed over a polycrystalline $La_{0.5}Sr_{0.5}MnO_{3-\delta}$ catalyst prepared by calcination at 950 °C. The excellent performance of the former can be related to the high Mn^{4+}/Mn^{3+} ratio, distinct oxygen nonstoichiometry, and single-crystalline structure of the catalyst.

1. Introduction

In the past two decades, researchers have been working on the synthesis and applications of perovskite-type oxides (ABO_3). Among the ABO_3 materials, those of the La–Mn–O family have been investigated intensively for catalytic applications. The La–Mn–O compounds show high level of oxygen mobility and thermal stability, and display stable oxidation states of the La and Mn elements [1]. An important aspect of this class of materials is that the compounds can be doped with other elements without having the ABO_3 structure significantly disturbed [2].

The physicochemical properties of the nanocrystalline materials are found to be distinctly different from those of their bulk counterparts [3]. Although there are many reports on the fabrication of nano- and micro-crystalline oxides [2,4–8], reports on the catalytic properties of the materials are rare. The main reason is that it is hard to achieve good size and morphology selectivity in the fabrication of the nanocrystals, especially in the generation of one-dimensional crystallites. It has been demonstrated that the materials with distinct morphology are superior to their irregular counterparts in catalytic performance [9–12]. The ABO_3 catalysts reported in the literature are mostly polycrystalline, and it is rare to come across single-crystalline ABO_3 in catalytic applications. Very recently, Teng et al. prepared $La_{0.5}Sr_{0.5}MnO_{3-\delta}$ microcubes hydrothermally. They observed good catalytic activity over the material in the combustion of methane, and attributed the outstanding performance to the unique structure and surface morphology of the single-crystallites [13]. In the past decade, we have prepared and characterized a large number of ABO_3 and perovskite-type halo-oxides; the catalytic performance of the materials was evaluated for the oxidation of carbon monoxide and/or light hydrocarbons [14]. Lately, we fabricated $La_{1-x}Sr_xMO_{3-\delta}$ (M = Mn, Co; $x = 0.4$–0.6) microrods, microcubes, and nanowires by means of direct hydrothermal synthesis [15,16]. In this paper, we report the generation of strontium-doped lanthanum manganite ($La_{1-x}Sr_xMnO_{3-\delta}$, $x = 0.4$, 0.5, and 0.6) microcubes via a template-free hydrothermal method. The crystallites show distinct morphology and exhibit excellent catalytic activity for toluene combustion.

2. Experimental

2.1. Catalyst preparation

For the synthesis of the $La_{1-x}Sr_xMnO_{3-\delta}$ ($x = 0.4$, 0.5, and 0.6) materials, 0.003 mol $KMnO_4$, 0.007 mol $MnCl_2{\cdot}4H_2O$, and

* Corresponding author. Tel.: +86 10 6739 6588; fax: +86 10 6739 1983.
** Co-Corresponding author. Tel.: +852 3411 7067; fax: +852 3411 7348.
E-mail addresses: hxdai@bjut.edu.cn (H. Dai), pctau@hkbu.edu.hk (C.T. Au).

1381-1169/$ – see front matter © 2008 Elsevier B.V. All rights reserved.
doi:10.1016/j.molcata.2008.10.006

stoichiometric amounts of lanthanum and strontium nitrates were dissolved in deionized water (total volume = 36 mL). Then 0.233, 0.290, and 0.350 mol of KOH was added, respectively, to the mixtures which were designated for the generation of the $La_{0.4}Sr_{0.6}MnO_{3-\delta}$, $La_{0.5}Sr_{0.5}MnO_{3-\delta}$, and $La_{0.6}Sr_{0.4}MnO_{3-\delta}$ samples. After ultrasonic treatment for 1 h, the mixtures were hydrothermally treated in 50-mL Teflon-lined stainless steel autoclaves at 250 °C (the pressure was 15–20 atm) for 50 h. The obtained substance (black in color) was washed several times with distilled water and dried at 120 °C overnight. For the purpose of comparison, we prepared also a polycrystalline $La_{0.5}Sr_{0.5}MnO_{3-\delta}$ catalyst (calcined at 950 °C for 4 h) by means of citric acid complexing [10]. All the chemicals and regents (analytical grade) were purchased from the Beijing Chemical Regent Company and used without further purification.

2.2. Chemical analysis for Mn^{4+} content

The content of Mn^{4+} was determined by having a sample digested in a known but excess amount of standard Mohr's salt ($Fe(NH_4)_2(SO_4)_2{\cdot}6H_2O$) solution that was acidified with 1.00 mol L^{-1} H_2SO_4; the excess amount of Fe^{2+} was back-titrated with 0.0167 mol L^{-1} $K_2Cr_2O_7$ in 3.00 mol L^{-1} HCl solution using 0.5% sodium diphenylamine sulfonate solution as indicator [17,18]. The experimental error in the determination of Mn^{4+} content was estimated to be ±0.10%.

2.3. Catalyst characterization

The crystal phases of the as-synthesized samples were determined on an X-ray diffractometer (XRD, Bruker/AXS D8 Advance) operated at 40 kV and 200 mA using Cu K_α radiation (λ = 0.15406 nm) and a nickel filter. The XRD patterns were recorded in the 2θ = 10–80° range. The specific surface areas of the samples were determined by means of N_2 adsorption at −196 °C on a Micromeritics ASAP 2020 apparatus with the samples outgassed at 250 °C for 2 h under vacuum prior to sample cooling and N_2 adsorption. The scanning electron microscopic (SEM) images of the samples were recorded on a JEOL JSM 6500F instrument also equipped for energy-dispersive X-ray (EDX) analysis (operated at 30 kV). The transmission electron microscopic (TEM) images and selected area electron diffraction (SAED) patterns were collected over a JEOL-2010 instrument (operated at 200 kV).

X-ray photoelectron spectroscopy (XPS, VG CLAM 4 MCD analyzer) was employed to determine the La 3d, Sr 2p, Mn 2p, O 1s, and C 1s binding energies (BE) of the surface entities of the as-synthesized samples using Mg K_α ($h\nu$ = 1253.6 eV) as excitation source. The instrumental resolution was 0.5 eV. After being treated in O_2 (flow rate = 20 mL min^{-1}) at 500 °C for 1 h (for the removal of surface carbonate and adsorbed water), the samples were cooled to room temperature (RT) and transferred into the spectrometer under helium (GLOVE BAG, Instruments for Research and Industry, USA). The above step guaranteed no exposure of the treated samples to air. The samples were then outgassed in the preparation chamber (10^{-5} Torr) for 0.5 h and introduced into the analysis chamber (3×10^{-9} Torr) for recording. The C 1s peak at 284.6 eV was taken as a reference for BE calibration.

For the O_2 temperature-programmed desorption (O_2-TPD) studies, the sample (0.1–0.2 g) was placed in the middle of a quartz microreactor of 8-mm inner diameter (i.d.). The outlet gases were analyzed on-line by mass spectrometry (Hiden HPR20). Before each run, the sample was treated in O_2 (flow rate = 20 mL min^{-1}) at 500 °C for 1 h, followed by cooling to RT in O_2 and helium purging (flow rate = 40 mL min^{-1}) for 4 h. The purpose of helium purging was to remove gas-phase oxygen in the system. The sample was then heated (10 °C min^{-1}) from RT to 900 °C. The amount of O_2 desorbed from the catalyst was quantified by calibrating the peak area against that of a standard O_2 pulse (50.0 μL).

Hydrogen temperature-programmed reduction (H_2-TPR) was carried out in the RT to 900 °C range with the sample (50 mg) placed in a quartz fixed-bed microreactor (i.d. = 6 mm). Before each run, the sample was treated in an O_2 flow (50 mL min^{-1}) at 500 °C for 1 h and then cooled down to RT under the same atmosphere. After being purged by N_2 (flow rate = 50 mL min^{-1}) for 30 min, the sample was reduced in a flow of 5% H_2/Ar (50 mL min^{-1}) at a heating rate of 10 °C min^{-1}. The effluent was monitored by a thermal conductivity detector (TCD). The thermal conductivity response was calibrated against the reduction of a known CuO powder sample (Aldrich, 99.995%).

2.4. Catalytic test

The catalytic activity was evaluated with the sample charged in a continuous flow fixed-bed quartz microreactor (i.d. = 8 mm). The catalyst (0.1–0.2 g, 40–60 mesh) was diluted with an equal amount of quartz sands (40–60 mesh). The reactant feed (flow rate = 33.3 mL min^{-1}) was 1000 ppm toluene + O_2 + N_2 (balance) with a toluene/O_2 molar ratio of 1/400, and space velocity of 20,000 h^{-1}. To change the space velocity and toluene/oxygen molar ratio, we altered the amount of catalyst and mass flow of oxygen, respectively. The outlet gases were analyzed on-line by a gas chromatograph (Shimadzu GC-2010) equipped with a flame ionization detector and a TCD, using a Chromosorb 101 column for toluene and a Carboxen 1000 column for permanent gas separation.

3. Results and discussion

3.1. Phase composition and surface morphology

The positions and relative intensities of the main XRD peaks of the $La_{1-x}Sr_xMnO_{3-\delta}$ catalysts (not shown) resemble those of $LaMnO_{3.15}$ (JCPDS PDF# 75-0440), indicating a cubic ABO_3 structure, in good agreement with the results reported by Teng et al. [13] and Gaudon et al. [19]. As reported by some researchers [19,20], the symmetry of the manganite structure is largely determined by the concentration of Mn^{4+} ions. For Sr-substituted manganite, Mn^{4+} concentration is governed by the level of Sr doping. The formation of the cubic phase at high Mn^{4+} contents has been attributed to the loss of Jahn–Teller distortion, and this loss can be related to the low Mn^{3+} level [19,21]. We also observed that with a decrease in levels of Sr^{2+} doping, there was an appearance of several weak signals that are ascribable to $La(OH)_3$. It is clear that the extent of La^{3+} substitution with Sr^{2+} has an effect on phase purity. The results of XRD investigation confirmed that the materials formed directly via the method of hydrothermal treatment without the need of high-temperature calcinations were cubic perovskite $La_{1-x}Sr_xMnO_{3-\delta}$.

Representative SEM and TEM images as well as SAED patterns of the $La_{1-x}Sr_xMnO_{3-\delta}$ samples are shown in Fig. 1. One can see that the $La_{0.4}Sr_{0.6}MnO_{3-\delta}$ sample contained aggregates (average size: 5–20 μm) of intertwined microcubes. The sighting of the "boat-shape" entities suggested hollow aggregates (Fig. 1(a–c)). Over the $La_{0.5}Sr_{0.5}MnO_{3-\delta}$ and $La_{0.6}Sr_{0.4}MnO_{3-\delta}$ samples, one can see interwoven structures with the microcubes "growing" in various directions, giving a sort of "leaf-like" spread with plenty of internal voids (Fig. 1(e and i)). In the case of the $La_{0.5}Sr_{0.5}MnO_{3-\delta}$ sample, there was a small quantity of individual microcubes (Fig. 1(g)). In the case of $La_{0.6}Sr_{0.4}MnO_{3-\delta}$, there were microcubes with the interior exposed (inset of Fig. 1(i)). From the SEM images, one can observe a small amount of "rod-shape" entities with diame-

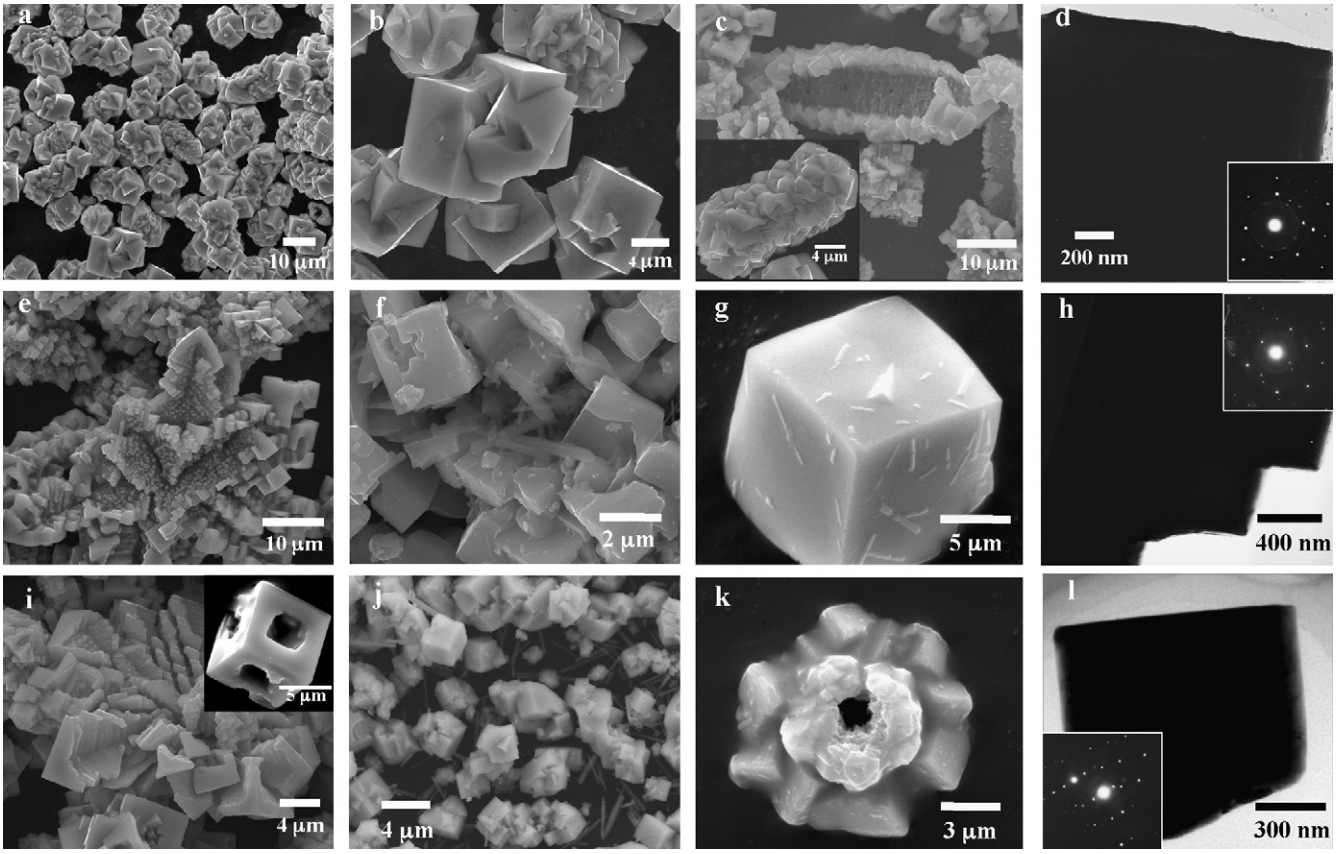

Fig. 1. SEM (a–c, e–g, and i–k) and TEM (d, h, and l) images as well as SAED patterns (insets) of $La_{0.4}Sr_{0.6}MnO_{3-\delta}$ (a–d), $La_{0.5}Sr_{0.5}MnO_{3-\delta}$ (e–h) and $La_{0.6}Sr_{0.4}MnO_{3-\delta}$ (i–l).

ter and length of 50–850 nm and 0.2–4.5 μm, respectively (Fig. 1(f and j)). The results of EDX analysis revealed that (i) there was no potassium in the fabricated samples (i.e. the as-obtained perovskite samples were $La_{1-x}Sr_xMnO_3$); (ii) the La:Sr:Mn atomic ratio of microcubes was 1.00:0.98:2.01, which was similar to the nominal La:Sr:Mn atomic ratio (0.5:0.5:1.0); (iii) the "rod-like" entities were mainly composed of La ions with a small amount of Mn and Sr ions, showing a La:Sr:Mn atomic ratio of 22.6:1:2.2. It is apparent that the microcubes are made up of $La_{0.5}Sr_{0.5}MnO_{3-\delta}$ while the microrods are composed of $La(OH)_3$, in agreement with the results of XRD investigation. The TEM images (Fig. 1(d, h, and l)) of the three samples also show the presence of microcubes. The corresponding SAED patterns revealed that the $La_{1-x}Sr_xMnO_{3-\delta}$ ($x = 0.4$–0.6) microcubes are single-crystalline. The sizes of the cubes are 5–25 μm for $La_{0.4}Sr_{0.6}MnO_{3-\delta}$, 0.6–8.5 μm for $La_{0.5}Sr_{0.5}MnO_{3-\delta}$, and 0.2–11 μm for $La_{0.6}Sr_{0.4}MnO_{3-\delta}$. It has been reported that factors such as metal precursors, ultrasonic treatment, and hydrothermal conditions (e.g. temperature, time, and pH value) could have an effect on the morphology of the as-synthesized products [2,4,22–24]. The $La_{1-x}Sr_xMnO_{3-\delta}$ samples fabricated in this study shows morphologies different from those of the $La_{0.5}Sr_{0.5}MnO_3$ nanowires reported by Zhu et al. [5] and Liu et al. [6]. It is possible that evolution of a particular morphology is determined by the mechanism of crystal growth [25,26].

3.2. Mn^{4+} content and structural defects of catalysts

The physical properties of the as-fabricated $La_{1-x}Sr_xMnO_{3-\delta}$ catalysts are summarized in Table 1. As expected, the bulk Mn^{4+}/Mn^{3+} ratio increased with a rise in x value due to charge compensation. It is generally accepted that La-rich $La_{1-x}Sr_xMnO_{3-\delta}$ samples display oxidative nonstoichiometry while Sr-rich ones display reductive nonstoichiometry [1,27]. According to the bulk Mn^{4+}/Mn^{3+} ratios and the principle of electroneutrality, the extent of oxygen nonstoichiometry (δ) was calculated at −0.012 for $La_{0.6}Sr_{0.4}MnO_{3-\delta}$, 0.015 for $La_{0.5}Sr_{0.5}MnO_{3-\delta}$, and 0.008 for $La_{0.4}Sr_{0.6}MnO_{3-\delta}$. Therefore, with x bigger than 0.4, the $La_{1-x}Sr_xMnO_{3-\delta}$ samples display a nonstoichiometry of oxygen-deficient nature, i.e. formation of oxygen vacancies. It is also observed that the BET surface areas of the three samples are $<3\ m^2\ g^{-1}$ (Table 1), in accordance with the microsize of $La_{1-x}Sr_xMnO_{3-\delta}$ microcubes.

The O 1s and Mn 2p XPS spectra of $La_{1-x}Sr_xMnO_{3-\delta}$ samples are shown in Fig. 2. There are signals at BE = 529.2 and 531.8 eV attributable to surface lattice oxygen (O^{2-}_{latt}) and adsorbed oxygen species O_{ads} (e.g. O^-, O_2^-, or O_2^{2-}), respectively [28–31]. The existence of hydroxyl and carbonate species on the surfaces can be excluded because the samples had been treated in an oxygen flow at 500 °C for 1 h and handled without being exposed to air

Table 1
Physical property of the $La_{1-x}Sr_xMnO_{3-\delta}$ catalysts.

x	Catalyst	Crystal phase	Mn^{4+}/Mn^{3+} (bulk)	δ	Surface area ($m^2\ g^{-1}$)
0.4	$La_{0.6}Sr_{0.4}MnO_{3-\delta}$	Cubic perovskite + $La(OH)_3$ (trace)	0.74	−0.012	1.8
0.5	$La_{0.5}Sr_{0.5}MnO_{3-\delta}$	Cubic perovskite + $La(OH)_3$ (trace)	0.89	0.015	1.8
0.6	$La_{0.4}Sr_{0.6}MnO_{3-\delta}$	Cubic perovskite	1.40	0.008	2.6

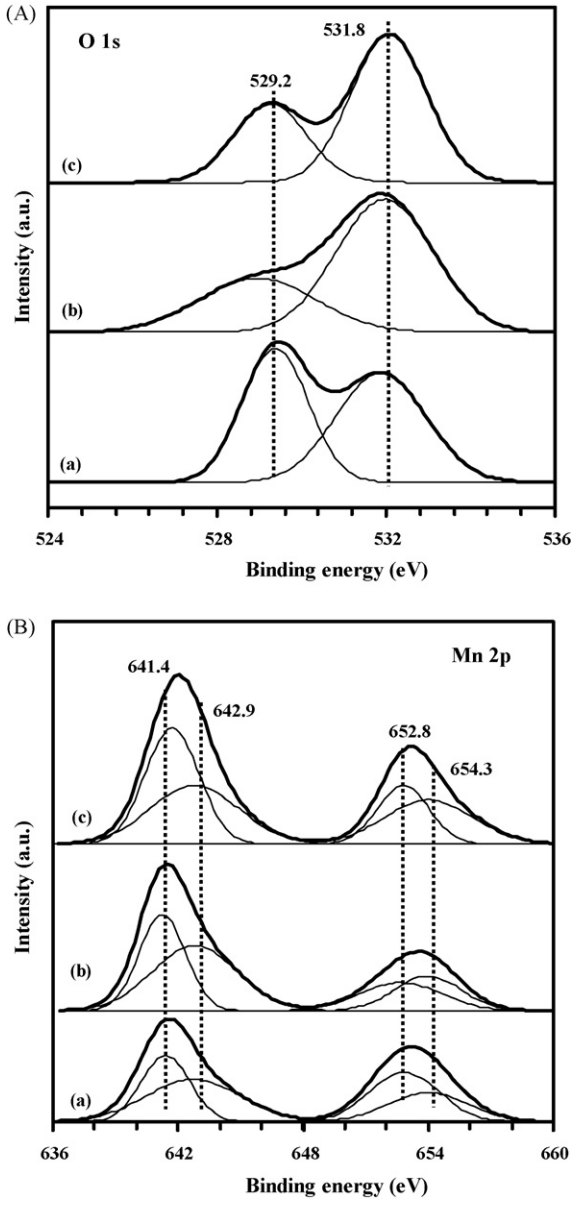

Fig. 2. (A) O 1s and (B) Mn 2p XPS spectra of (a) $La_{0.4}Sr_{0.6}MnO_{3-\delta}$, (b) $La_{0.5}Sr_{0.5}MnO_{3-\delta}$, and (c) $La_{0.6}Sr_{0.4}MnO_{3-\delta}$.

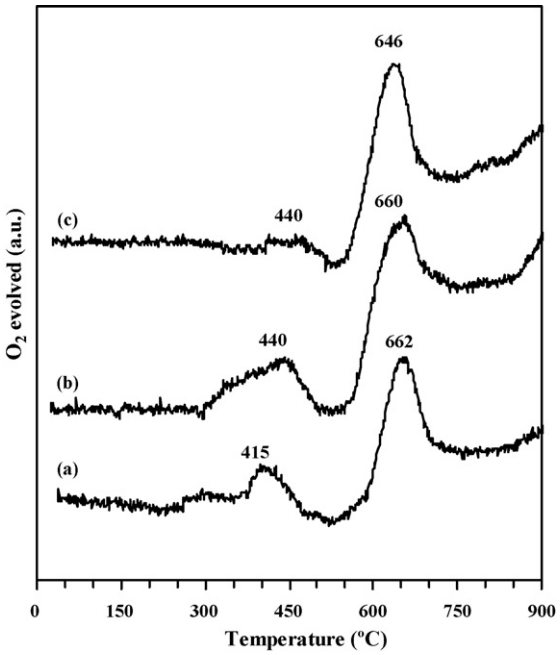

Fig. 3. O_2-TPD profiles of (a) $La_{0.4}Sr_{0.6}MnO_{3-\delta}$, (b) $La_{0.5}Sr_{0.5}MnO_{3-\delta}$, and (c) $La_{0.6}Sr_{0.4}MnO_{3-\delta}$.

prior to XPS measurement. Usually, a rise in Sr^{2+}-doping level of $La_{1-x}Sr_xMnO_{3-\delta}$ would result in an increase in oxygen deficiency. Nevertheless, due to the leaching of La from $La_{1-x}Sr_xMnO_{3-\delta}$ (La ended up as $La(OH)_3$), there was in fact a decline in oxygen deficiency. With a rise in levels of Sr^{2+} doping, the O_{ads}/O^{2-}_{latt} ratio comes to its highest at $x = 0.5$ (Table 2), indicating that among the three samples, $La_{0.5}Sr_{0.5}MnO_{3-\delta}$ possesses the highest amount of O_{ads}. From Fig. 2(B), one can observe two asymmetrical signals at BE = ca. 641.5 and 653.5 eV assignable to Mn $2p_{3/2}$ and Mn $2p_{1/2}$, respectively [32]. The Mn $2p_{3/2}$ peak can be deconvoluted into two components at BE = 641.4 and 642.9 eV whereas the Mn $2p_{1/2}$ peak into two components at BE = 652.8 and 654.3 eV. The components at BE = 641.4 and 652.8 eV can be assigned to Mn^{3+} ions, while those at BE = 642.9 and 654.3 eV to Mn^{4+} ions [32]. An estimation of relative signal intensity of Mn^{3+} and Mn^{4+} reveals that the $La_{0.5}Sr_{0.5}MnO_{3-\delta}$ sample contains the highest amount of surface Mn^{4+} (Table 2). According to the surface compositions calculated based on the XPS results (Table 2), one can see that there is Mn enrichment on the surfaces, in concordance with results reported by other researchers [33,34]. In the cases of the $La_{0.6}Sr_{0.4}MnO_{3-\delta}$ and $La_{0.5}Sr_{0.5}MnO_{3-\delta}$ samples, the surface Mn^{4+}/Mn^{3+} ratio is higher than the bulk Mn^{4+}/Mn^{3+} ratio whereas in the case of the $La_{0.4}Sr_{0.6}MnO_{3-\delta}$ sample, the bulk Mn^{4+}/Mn^{3+} ratio is higher than the surface Mn^{4+}/Mn^{3+} ratio. It is worth pointing out that due to the existence of the $La(OH)_3$ phase and the possible presence of certain phases that are undetectable by the XRD technique, the oxygen vacancy densities of the $La_{1-x}Sr_xMnO_{3-\delta}$ samples could be higher than those calculated from the Mn^{4+} content.

3.3. Oxygen species and reducibility of catalysts

The O_2-TPD profiles of the $La_{1-x}Sr_xMnO_{3-\delta}$ samples are shown in Fig. 3. There are three peaks for each sample. The first one locates between 250 and 525 °C, the second one is located between 525 and 800 °C, and the third one starts from ca. 800 °C. The amount of oxygen desorption in the 250–525 °C range is estimated to be 40.2, 56.0, and 15.0 μmol g^{-1}_{cat} whereas that in the 525–800 °C range to be 124.6, 137.3, and 120.8 μmol g^{-1}_{cat} for the samples with $x = 0.6$, 0.5,

Table 2
Surface molar compositions of the $La_{1-x}Sr_xMnO_{3-\delta}$ catalysts based on XPS results.

Catalyst	La/Mn	Sr/Mn	La/Sr	Mn/(La + Sr + Mn + O)	O_{ads}/O^{2-}_{latt}	Mn^{4+}/Mn^{3+}
$La_{0.6}Sr_{0.4}MnO_{3-\delta}$	0.54 (0.6)[a]	0.28 (0.4)	1.89 (1.5)	0.34 (0.2)	1.82	0.98
$La_{0.5}Sr_{0.5}MnO_{3-\delta}$	0.11 (0.5)	0.15 (0.5)	0.71 (1.0)	0.50 (0.2)	2.05	1.16
$La_{0.4}Sr_{0.6}MnO_{3-\delta}$	0.30 (0.4)	0.37 (0.6)	0.81 (0.67)	0.43 (0.2)	1.11	0.96

[a] The data in parentheses are based on the nominal values.

and 0.4, respectively. According to Seiyama [35], the peaks in the range of 250–525 °C could be ascribed to α desorption originating from O_{ads} located at oxygen vacancies. Thus, the signal intensity of α desorption can provide a rough estimation of amount of oxygen vacancies on the surface of the samples. Based on the amount of oxygen desorption in the 250–525 °C range, we deduce that the surface density of oxygen vacancies of the three catalysts decreases in order of $La_{0.5}Sr_{0.5}MnO_{3-\delta}$ > $La_{0.4}Sr_{0.6}MnO_{3-\delta}$ > $La_{0.6}Sr_{0.4}MnO_{3-\delta}$. It is generally accepted that β desorption (desorption of surface O^{2-}_{latt}) of Mn-based perovskites occurs above 500 °C. Nonetheless, it seems that it is not easy to exclude the possible contribution of the bulk oxygen species [35–38]. In any case, the occurrence of β desorption should result in partial reduction of the Mn-based perovskites. We estimate that the amount of oxygen desorption in the 500–750 °C range over the $La_{0.5}Sr_{0.5}MnO_{3-\delta}$, $La_{0.4}Sr_{0.6}MnO_{3-\delta}$, and $La_{0.6}Sr_{0.4}MnO_{3-\delta}$ catalyst is 137.3, 124.6, and 120.8 μmol g^{-1}_{cat}, respectively. In other words, the extent of β desorption is the highest over the $La_{0.5}Sr_{0.5}MnO_{3-\delta}$ sample, and those over $La_{0.4}Sr_{0.6}MnO_{3-\delta}$ and $La_{0.6}Sr_{0.4}MnO_{3-\delta}$ samples are rather similar. From Table 2, one can see that the surface Mn^{4+}/Mn^{3+} ratios of the three catalysts show a similar pattern, with that of $La_{0.5}Sr_{0.5}MnO_{3-\delta}$ (1.16) being the highest followed by $La_{0.6}Sr_{0.4}MnO_{3-\delta}$ (0.98) and $La_{0.4}Sr_{0.6}MnO_{3-\delta}$ (0.96), which are similar to each other (Table 2). One can also see in Table 1 that the bulk Mn^{4+}/Mn^{3+} ratio of $La_{0.5}Sr_{0.5}MnO_{3-\delta}$, $La_{0.4}Sr_{0.6}MnO_{3-\delta}$, and $La_{0.6}Sr_{0.4}MnO_{3-\delta}$ is 0.89, 1.40, and 0.74, respectively. It is apparent that the β desorption of the three catalysts correlate better with the nature of the catalysts in terms of surface Mn^{4+}/Mn^{3+} ratios.

Irusta et al. reported that the partial substitution of La^{3+} for Sr^{2+} in Mn-based perovskites would promote Mn^{4+} reduction [39]. The three Sr-substituted perovskites show discrepancy in the Mn oxidation state and oxygen nonstoichiometry, and it is expected that they are different in reducibility and oxygen transport properties. Fig. 4(A) shows the H_2-TPR profiles of the $La_{1-x}Sr_xMnO_{3-\delta}$ samples. Over the $La_{0.4}Sr_{0.6}MnO_{3-\delta}$ sample, the signals at 410 and 760 °C correspond to a H_2 consumption of 2.34 and 1.08 mmol g^{-1}_{cat}. The reduction bands at 430 and 732 °C (the latter shows a shoulder at 771 °C) acquired over the $La_{0.5}Sr_{0.5}MnO_{3-\delta}$ sample represent a H_2 consumption of 2.46 and 0.92 mmol g^{-1}_{cat}, respectively. Over the $La_{0.6}Sr_{0.4}MnO_{3-\delta}$ sample, the intensity of the 462 and 733 °C peaks corresponds to a H_2 consumption of 2.32 and 0.95 mmol g^{-1}_{cat}.

Theoretically, if the reduction of the $La_{1-x}Sr_xMnO_{3-\delta}$ samples with x = 0.6, 0.5, and 0.4 corresponded to the change from Mn^{4+} to Mn^{2+}, the amount of H_2 consumed would be 4.74, 4.63, and 45.2 mmol g^{-1}_{cat}, respectively; if the reduction corresponded to the change from Mn^{3+} to Mn^{2+}, the amount of H_2 consumed would be 2.37, 2.31, and 2.26 mmol g^{-1}_{cat}. The H_2-TPR results indicated that total H_2 consumption was 3.42, 3.38, and 3.27 mmol g^{-1}_{cat} over the $La_{1-x}Sr_xMnO_{3-\delta}$ samples (x = 0.6, 0.5, and 0.4), respectively, and the values are only slightly lower than the corresponding theoretical values (3.58, 3.40, and 3.37 mmol g^{-1}_{cat}) estimated according to the bulk Mn^{4+}/Mn^{3+} ratios (Table 1). The molar ratio of consumed H_2 to Mn was calculated at 0.72, 0.73, and 0.72 for the $La_{1-x}Sr_xMnO_{3-\delta}$ samples (x = 0.6, 0.5, and 0.4), respectively. Since these values are higher than 0.50, we are sure that both Mn^{4+} and Mn^{3+} are present in the samples [36], as evidenced by the results of chemical analysis (Table 1) and XPS investigation (Fig. 2(B)).

It is apparent that with a rise in the extent of Sr^{2+} substitution, there is an increase in reducibility. However, this increase in reducibility cannot be conclusive. It is known that the small crystallites of manganese oxides (not detectable by the XRD technique) are more reducible than the Mn-based perovskites [36]. The results of XPS investigation suggested Mn enrichment on the surface (Table 2), and it is possible that there were small crystallites of manganese oxides on the $La_{1-x}Sr_xMnO_{3-\delta}$ samples. According

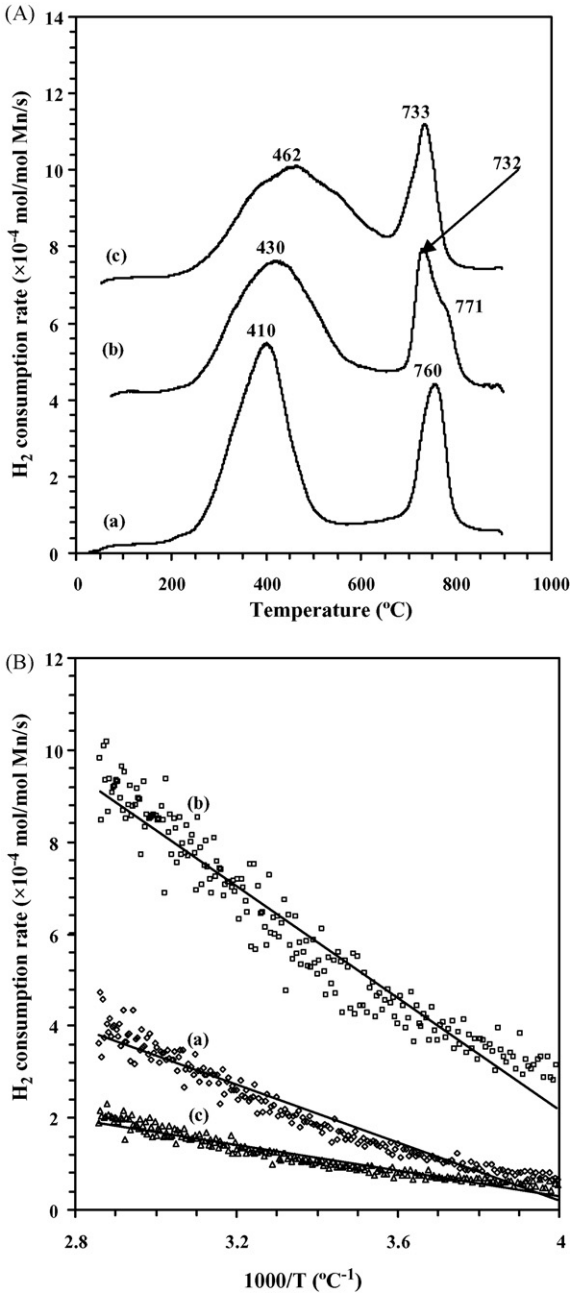

Fig. 4. (A) H_2-TPR profiles and (B) initial hydrogen consumption rate of (a) $La_{0.4}Sr_{0.6}MnO_{3-\delta}$, (b) $La_{0.5}Sr_{0.5}MnO_{3-\delta}$, and (c) $La_{0.6}Sr_{0.4}MnO_{3-\delta}$.

to findings of Ponce et al. [33] and those of ours [40], we assign the low-temperature reduction signal to the reduction of Mn^{4+} to Mn^{3+} as well as the removal of oxygen adspecies located at the oxygen vacancies, and the high-temperature reduction signal to the reduction of Mn^{3+} to Mn^{2+}. The amount of H_2 consumption estimated based on the low-temperature reduction band of $La_{0.5}Sr_{0.5}MnO_{3-\delta}$, $La_{0.4}Sr_{0.6}MnO_{3-\delta}$, and $La_{0.6}Sr_{0.4}MnO_{3-\delta}$ is 2.46, 2.34, and 2.32 mmol g^{-1}_{cat}, respectively. It has been pointed out by Machocki et al. that factors such as high oxygen vacancy density and high Mn^{4+} concentration are beneficial for the catalytic combustion of hydrocarbons [34]. The amount of H_2 consumed in the temperature range of 250–350 °C stands for 23.6, 26.0, and 13.3% of the total H_2 consumption detected over the samples with x = 0.6, 0.5, and 0.4, respectively. For better understanding of the reducibil-

Table 3
Catalytic activities of $La_{1-x}Sr_xMnO_{3-\delta}$ samples for toluene complete oxidation.

$T_{x\%}$ (x% = toluene conversion)	Catalysts			
	Single-crystalline $La_{0.6}Sr_{0.4}MnO_{3-\delta}$	Single-crystalline $La_{0.5}Sr_{0.5}MnO_{3-\delta}$	Single-crystalline $La_{0.4}Sr_{0.6}MnO_{3-\delta}$	Polycrystalline $La_{0.5}Sr_{0.5}MnO_{3-\delta}$
$T_{10\%}$ (°C)	241	209	218	245
$T_{50\%}$ (°C)	299	250	255	296
$T_{100\%}$ (°C)	310	255	260	368

ity of the three samples, we obtained the initial H_2 consumption rate of low-temperature reduction (Fig. 4(B)). It is apparent that the $La_{0.5}Sr_{0.5}MnO_{3-\delta}$ sample exhibits the highest reduction rate while $La_{0.6}Sr_{0.4}MnO_{3-\delta}$ shows the lowest. In other words, the order of the total amount of oxygen vacancies and Mn^{4+} in the three catalysts agrees well with that of the reduction rate. As will be demonstrated in the next section, the catalytic performance of the single-crystalline ABO_3 materials follows a similar order.

3.4. Catalytic performance

Table 3 shows the catalytic activities of the $La_{1-x}Sr_xMnO_{3-\delta}$ samples for total oxidation of toluene under the conditions of toluene concentration = 1000 ppm, toluene/O_2 molar ratio = 1/400, and space velocity = 20,000 h^{-1}. The $T_{x\%}$ is defined as the temperature for the toluene conversion of x%. From Table 3, one can see that the temperature difference from $T_{10\%}$ to $T_{50\%}$ was 40–50 °C over all the catalysts, whereas that from $T_{50\%}$ to $T_{100\%}$ was only 5–10 °C over the single-crystalline catalysts and 72 °C over the polycrystalline catalyst. The phenomenon of a sudden rise in toluene conversion within a small range of temperature over the single-crystalline catalysts is rather similar to that over the Pt catalyst [41]. Apparently, the single-crystalline $La_{0.5}Sr_{0.5}MnO_{3-\delta}$ catalyst performed better than its polycrystalline counterpart. Considering the fact that the surface area (1.8 $m^2\,g^{-1}$) of the single-crystalline $La_{0.5}Sr_{0.5}MnO_{3-\delta}$ catalyst was lower than that of its polycrystalline counterpart (5.3 $m^2\,g^{-1}$), one can ascribe the discrepancy in activity to the difference in oxygen nonstoichiometry and redox ability as well as the crystal nature. In terms of increasing catalytic activity, the catalysts followed a sequence of $La_{0.5}Sr_{0.5}MnO_{3-\delta} > La_{0.4}Sr_{0.6}MnO_{3-\delta} \gg La_{0.6}Sr_{0.4}MnO_{3-\delta}$. The $La_{0.5}Sr_{0.5}MnO_{3-\delta}$ ($T_{100\%}$ = 255 °C at space velocity = 20,000 h^{-1}) and $La_{0.4}Sr_{0.6}MnO_{3-\delta}$ ($T_{100\%}$ = 260 °C at space velocity = 20,000 h^{-1}) catalysts outperform the $LaMnO_3$ and $La_{0.8}Sr_{0.2}MnO_3$ catalysts over which $T_{100\%}$ was found to be above 340 °C even at a low space velocity of 184 h^{-1} [39]. The catalytic performance of $La_{0.5}Sr_{0.5}MnO_{3-\delta}$ and $La_{0.4}Sr_{0.6}MnO_{3-\delta}$ is comparable to that of the widely investigated Pt catalyst [41]. The trends of specific reaction rate (reaction rate normalized by surface area) versus reaction temperature (not shown) were similar to that of toluene conversion versus reaction temperature over our single-crystalline catalysts. The results implied that the surface area of $La_{1-x}Sr_xMnO_{3-\delta}$ is not a determining factor for toluene combustion. It is worth pointing out that the products detected were essentially CO_2 and H_2O as confirmed by the estimated carbon balance of 99.5%.

It is generally believed that the catalytic activity of ABO_3 materials can be related to (i) oxidation states of transition metal ions, (ii) amount of nonstoichiometric oxygen, and (iii) the structural defects of the materials [1,35]. Based on the results of Machocki et al. [34], Lisi et al. [42], and the results of the present study, we suggest that the catalytic activities of $La_{1-x}Sr_xMnO_{3-\delta}$ catalysts could be related to the nature of the redox processes: $Mn^{4+} \Leftrightarrow Mn^{3+}$. In other words, the catalytic performance of the catalysts is determined by surface as well as by bulk Mn^{4+}/Mn^{3+} ratios. Machocki et al. [34] reported that the rate of methane oxidation over $LaMnO_3$ displays a linear relationship with the surface Mn^{4+}/Mn^{3+} ratio. Furthermore, it has been pointed out by Chakrabarty and Rao [43] and reiterated by Teng et al. [13] that M^{3+}–O–M^{4+} entities on the surface or near the surface of $La_{1-x}Sr_xMO_{3-\delta}$ (M = Mn, Co) could have an impact on catalytic activity. A rise in the Mn oxidation state could promote redox action in which Mn is partially reduced in the course of providing the reaction with oxygen, and then the reduced Mn is reoxidized via the intake of oxygen from the gas phase. It has been shown in Section 3.2 that the bulk Mn^{4+}/Mn^{3+} ratios of the catalysts decrease in order of $La_{0.4}Sr_{0.6}MnO_{3-\delta} > La_{0.5}Sr_{0.5}MnO_{3-\delta} > La_{0.6}Sr_{0.4}MnO_{3-\delta}$ (Table 1) whereas the surface Mn^{4+}/Mn^{3+} ratio follows a sequence of $La_{0.5}Sr_{0.5}MnO_{3-\delta} > La_{0.4}Sr_{0.6}MnO_{3-\delta} \approx La_{0.6}Sr_{0.4}MnO_{3-\delta}$ (Table 2). By comparing the order of catalytic performance to that of surface and bulk Mn^{4+}/Mn^{3+} ratios, one can see that the order of catalytic activity is similar to that of the surface Mn^{4+}/Mn^{3+} ratios. In other words, the surface Mn^{4+}/Mn^{3+} ratio of the $La_{1-x}Sr_xMnO_{3-\delta}$ catalysts is a dominating factor that influences the catalytic activity.

Apart from Mn^{4+}/Mn^{3+} ratios, catalytic activity is often discussed in terms of mobility of lattice oxygen as related to the reducibility of transition metals in the matrixes of perovskites [44,45]. By comparing the temperatures for maximum reduction (T_{max}) in the low-temperature range shown in Fig. 4(A), one can see that an increase in the Sr content would lead to a decrease in T_{max}. As far as low-temperature reduction is concerned, reducibility of the catalysts decreases according to the sequence of $La_{0.4}Sr_{0.6}MnO_{3-\delta} > La_{0.5}Sr_{0.5}MnO_{3-\delta} > La_{0.6}Sr_{0.4}MnO_{3-\delta}$. It was pointed out by Nakamura et al. [46] that during the oxidation of CO over $La_{1-x}Sr_xCoO_{3-\delta}$ catalysts, the involvement of lattice oxygen, reduction of transition metal ions, and formation of oxygen vacancies occur concurrently. The role of oxygen vacancies is to enhance the rate of O_2 dissociation on the surface and to increase mobility of O^{2-}_{latt} [38,44]. It has been reported that the presence of oxygen vacancies could result in promotion of oxygen diffusion and enhancement of O^{2-}_{latt} mobility [40,44]. As revealed in Fig. 3, the amount of oxygen vacancies on the $La_{1-x}Sr_xMnO_{3-\delta}$ catalysts followed the order of $La_{0.5}Sr_{0.5}MnO_{3-\delta} > La_{0.4}Sr_{0.6}MnO_{3-\delta} > La_{0.6}Sr_{0.4}MnO_{3-\delta}$, which is similar to the order of the total amount of oxygen vacancies and Mn^{4+} (Table 1 and Fig. 4). These results suggested that the $La_{0.5}Sr_{0.5}MnO_{3-\delta}$ catalyst contains more oxygen vacancies in the bulk than $La_{0.4}Sr_{0.6}MnO_{3-\delta}$. It should be noted that a small amount of $La(OH)_3$ nanorods are formed during the synthesis of $La_{0.6}Sr_{0.4}MnO_{3-\delta}$ and $La_{0.5}Sr_{0.5}MnO_{3-\delta}$. Due to formation of $La(OH)_3$, the genuine oxygen nonstoichiometry (δ) could be bigger than that estimated according to the nominal metal compositions and the titration results of Mn^{4+} determination.

The effects of space velocity and toluene/oxygen molar ratio on the catalytic performance of $La_{0.4}Sr_{0.6}MnO_{3-\delta}$ were examined (Fig. 5). As expected, the catalytic activity decreases at elevated space velocities (Fig. 5(A)). At 5000 h^{-1}, the values of $T_{50\%}$ and $T_{100\%}$ are 210 and 220 °C, respectively. Further rise in the space velocity from 5000 to 40,000 h^{-1} would result in a marked decline in the activity. From Fig. 5(B), one can see that when the toluene/O_2 molar ratio is changed from 1/100 to 1/400 (i.e. a rise in the O_2 con-

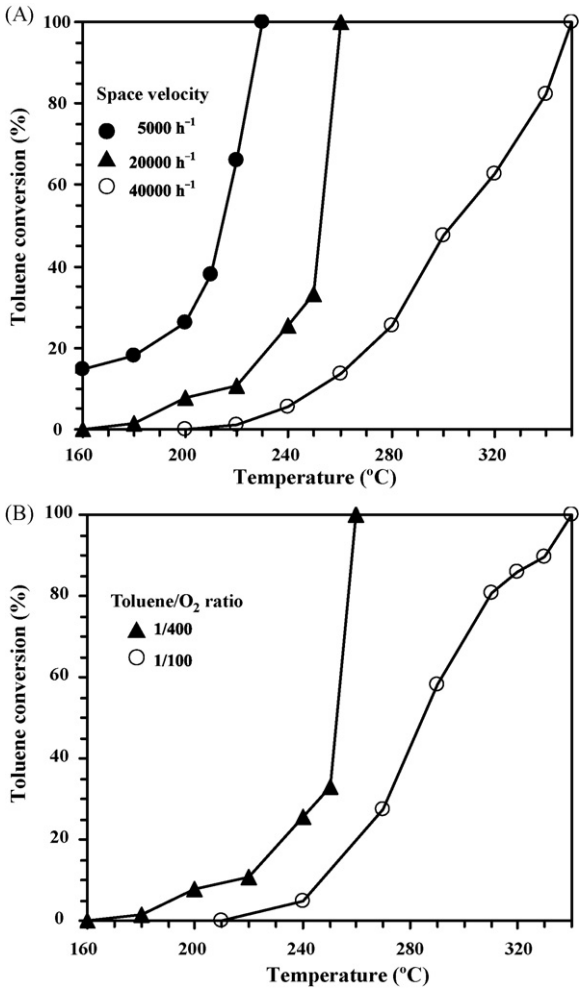

Fig. 5. Effects of (A) space velocity (at toluene/O_2 molar ratio = 1/400) and of (B) toluene/O_2 molar ratio (at space velocity = 20,000 h^{-1}) on the catalytic activity of $La_{0.4}Sr_{0.6}MnO_{3-\delta}$.

tent), $T_{100\%}$ declined from 340 to 260 °C (i.e. an increase in activity). It is clear that the O_{ads} species plays an important role in complete oxidation of toluene. It was proposed by Voorhoeve et al. [47] that oxidation reactions over ABO_3 can be classified into two types: (i) intrafacial reactions in which O^{2-}_{latt} acts as active species; and (ii) suprafacial reactions in which O_{ads} acts as active species. The suprafacial reactions are believed to proceed at temperature lower than that of the intrafacial reactions. Kremenic et al. studied the combustion of propylene and *iso*butene at 300 °C over $LaBO_3$ (B = Cr, Mn, Fe, Co, Ni) catalysts and suggested that reactions took place according to the suprafacial mechanism [48]. In this present study, the complete conversion of toluene occurs below 320 °C over the $La_{1-x}Sr_xMnO_{3-\delta}$ catalysts, suggesting that the combustion of toluene proceeds via the suprafacial mechanism. It is known that oxidation of hydrocarbons involving O_{ads} depends greatly on partial pressure of oxygen in the reactant feed [35]. We observed that the catalytic activity of $La_{0.4}Sr_{0.6}MnO_{3-\delta}$ increases with a rise in O_2 partial pressure (i.e. a drop in toluene/O_2 molar ratio) (Fig. 5(B)). The phenomenon reiterates that O_{ads} species are essential for complete combustion of toluene over the $La_{1-x}Sr_xMnO_{3-\delta}$ catalysts.

4. Conclusion

Single-crystalline $La_{1-x}Sr_xMnO_{3-\delta}$ perovskite microcubes have been synthesized from a mixture of $KMnO_4/MnCl_2$ (molar ratio = 3/7) and stoichiometric amounts of lanthanum and strontium nitrates in an aqueous KOH medium via a facile hydrothermal approach (250 °C for 50 h). The main phase of the as-prepared catalysts is cubic perovskite. Depending on the extent of Sr doping and the concentration of KOH, the samples show various forms of microcubes, and a trace amount of $La(OH)_3$. The approach is believed to be applicable to the synthesis of other ABO_3 compounds. The fabricated $La_{1-x}Sr_xMnO_{3-\delta}$ catalysts display different states of oxygen nonstoichiometry. The total amount of oxygen vacancies and Mn^{4+} in the catalysts follows the order of $La_{0.5}Sr_{0.5}MnO_{3-\delta} > La_{0.4}Sr_{0.6}MnO_{3-\delta} > La_{0.6}Sr_{0.4}MnO_{3-\delta}$. We observed that the trends of catalyst reducibility and catalytic performance of the three catalysts follow a similar order. The single-crystalline manganite materials display high levels of catalytic activity for toluene combustion, and among the three fabricated catalysts, the $La_{0.5}Sr_{0.5}MnO_{3-\delta}$ catalyst performed the best. Under reaction conditions of toluene concentration = 1000 ppm, toluene/O_2 molar ratio = 1/400, and space velocity = 20,000 h^{-1}, toluene conversion is 100% at 255 °C over $La_{0.5}Sr_{0.5}MnO_{3-\delta}$. It is deduced that the good performance of the $La_{1-x}Sr_xMnO_{3-\delta}$ catalysts can be related to the Mn^{4+}/Mn^{3+} redox couple, the single-crystalline structure, and the surface oxygen vacancies of the $La_{1-x}Sr_xMnO_{3-\delta}$ materials.

Acknowledgments

This work was supported by the Natural Science Foundation of Beijing Municipality (Key Class B project of grant number KZ200610005004) and Funding Project for Academic Human Resources Development in Institutions of Higher Learning under the Jurisdiction of Beijing Municipality (PHR (IHLB)). C.T.A. thanks the RGC, Hong Kong Special Administration Region for financial support (Grant HKBU 200106).

References

[1] M.A. Peña, J.L.G. Fierro, Chem. Rev. 101 (2001) 1981–2018.
[2] J.J. Urban, L. Ouyang, M. Jo, D.S. Wang, H. Park, Nano Lett. 4 (2004) 1547–1550.
[3] A.P. Alivisatos, Science 271 (1996) 933–937.
[4] C.G. Hu, H. Liu, C.S. Lao, L.Y. Zhang, D. Davidovic, Z.L. Wang, J. Phys. Chem. B 110 (2006) 14050–14054.
[5] D. Zhu, H. Zhu, Y.H. Zhang, J. Phys. Condens. Matter 14 (2002) L519–L524.
[6] J. Liu, H. Wang, M. Zhu, B. Wang, H. Yan, Mater. Res. Bull. 38 (2003) 817–822.
[7] P. Yang, T. Deng, D. Zhao, P. Feng, D. Pine, B.F. Chmelka, G.M. Whitesides, G.D. Stucky, Science 282 (1998) 2244–2246.
[8] J. Spooren, A. Rumpecker, F. Millange, R.I. Walton, Chem. Mater. 15 (2003) 1401–1403.
[9] L.G. Tejuca, J.L.G. Fierro, J.M.D. Tascon, Adv. Catal. 36 (1989) 237–328.
[10] S. Royer, F. Bérubé, S. Kaliaguine, Appl. Catal. A 282 (2005) 273–284.
[11] J.R. Niu, J.G. Deng, W. Liu, L. Zhang, G.Z. Wang, H.X. Dai, H. He, X.H. Zi, Catal. Today 126 (2007) 420–429.
[12] G. Sinquin, C. Petit, J.P. Hindermann, A. Kiennemann, Catal. Today 70 (2001) 183–196.
[13] F. Teng, W. Han, S. Liang, B. Gaugeu, R. Zong, Y. Zhu, J. Catal. 250 (2007) 1–11.
[14] H.X. Dai, C.T. Au, Curr. Top. Catal. 3 (2002) 33–80.
[15] H.X. Dai, J.G. Deng, Y. Zhang, H. He, X.H. Zi, Chin. Patent CN1974886, Beijing University of Technology, 2006.
[16] H.X. Dai, J.G. Deng, Y. Zhang, H. He, X.H. Zi, Chin. Patent CN1974887, Beijing University of Technology, 2006.
[17] R. Spinicci, M. Faticanti, P. Marini, S. De Rossi, P. Porta, J. Mol. Catal. A 197 (2003) 147–155.
[18] Y. Wu, T. Yu, B.S. Dou, C.X. Wang, X.F. Xie, Z.L. Yu, S.R. Fan, Z.R. Fan, L.C. Wang, J. Catal. 120 (1989) 88–107.
[19] M. Gaudon, C. Laberty-Robert, F. Ansart, P. Stevens, A. Rousset, Solid State Sci. 4 (2002) 125–133.
[20] A. Chakraborty, S.P. Devi, S. Roy, H.S. Maiti, Mater. Lett. 20 (1994) 63–69.
[21] A. Wold, R.J. Arnott, J. Phys. Chem. Solids 9 (1959) 176–180.
[22] X. Wang, Y. Li, Angew. Chem. Int. Ed. 41 (2002) 4790–4793.
[23] S.M. Lee, S.N. Cho, J.W. Cheon, Adv. Mater. 15 (2003) 441–444.
[24] W. Jiang, X. Gong, Z. Chen, Y. Hu, X. Zhang, X. Gong, Ultrason. Sonochem. 14 (2007) 208–212.
[25] H.C. Zeng, J. Feng, Chem. Mater. 15 (2003) 2829–2835.
[26] R. Xu, H.C. Zeng, J. Phys. Chem. B 107 (2003) 926–930.
[27] L. Rørmark, K. Wiik, S. Stølen, T. Grande, J. Mater. Chem. 12 (2002) 1058–1067.

[28] A.F. Carley, M.W. Roberts, A.K. Santra, J. Phys. Chem. B 101 (1997) 9978–9983.
[29] N. Yamazoe, Y. Teraoka, T. Seiyama, Chem. Lett. 10 (1981) 1767–1770.
[30] J.L.G. Fierro, L.G. Tejuca, Appl. Surf. Sci. 27 (1987) 453–457.
[31] G. Fierro, M. Lo Jacono, M. Inversi, R. Dragone, P. Porta, Top. Catal. 10 (2000) 39–48.
[32] J.F. Moulder, W.F. Stickle, P.E. Sobol, K.D. Bomben, in: J. Chastain, R.C. King Jr. (Eds.), Handbook of X-Ray Photoelectron Spectroscopy, Physical Electronics, Inc., Eden Prairie, 1995, pp. 78–79.
[33] S. Ponce, M.A. Peña, J.L.G. Fierro, Appl. Catal. B 24 (2000) 193–205.
[34] A. Machocki, T. Ioannides, B. Stasinska, W. Gac, G. Avgouropoulos, D. Delimaris, W. Grzegorczyk, S. Pasieczna, J. Catal. 227 (2004) 282–296.
[35] T. Seiyama, in: L.G. Tejuca, J.L.G. Fierro (Eds.), Properties and Applications of Perovskite-Type Oxides, Marcel Dekker, New York, 1993, pp. 215–234.
[36] P. Ciambelli, S. Cimino, S. De Rossi, M. Faticanti, L. Lisi, G. Minelli, I. Pettiti, P. Porta, G. Russo, M. Turco, Appl. Catal. B 24 (2000) 243–253.
[37] N.A. Merino, B.P. Barbero, P. Grange, L.E. Cadús, J. Catal. 231 (2005) 232–244.
[38] R. Zhang, A. Villanueva, H. Alamdari, S. Kaliaguine, J. Mol. Catal. A 258 (2006) 22–34.
[39] S. Irusta, M.P. Pina, M. Menéndez, J. Santamaría, J. Catal. 179 (1998) 400–412.
[40] H.X. Dai, H. He, P.H. Li, L.Z. Gao, C.T. Au, Catal. Today 90 (2004) 231–244.
[41] J. Blanco, A.L. Petre, M. Yates, M.P. Martin, J.A. Martin, M.A. Martin-Luengo, Appl. Catal. B 73 (2007) 128–134.
[42] L. Lisi, G. Bagnasco, P. Ciambelli, S. De Rossi, P. Porta, G. Russo, M. Turco, J. Solid State Chem. 146 (1999) 176–183.
[43] D.K. Chakrabarty, D.Y. Rao, React. Kinet. Catal. Lett. 33 (1987) 131–136.
[44] S. Royer, H. Alamdari, D. Duprez, S. Kaliaguine, Appl. Catal. B 58 (2005) 273–288.
[45] S. Royer, D. Duprez, S. Kaliaguine, J. Catal. 234 (2005) 364–375.
[46] T. Nakamura, M. Misono, Y. Yoneda, Chem. Lett. 10 (1981) 1589–1592.
[47] R.J.H. Voorhoeve, J.P. Remeika, P.E. Freeland, B.T. Mathias, Science 177 (1972) 353–354.
[48] G. Kremenic, J.M.L. Nieto, J.M.D. Tascon, L.G. Tejuca, J. Chem. Soc., Faraday Trans. 1 81 (1985) 939–949.